A SEISMOLOGICAL INTERPRETATION OF

THE FOURIER AMPLITUDE SPECTRUM

OF GROUND ACCELERATION[1]

by

H.S. Hasegawa

Department of Energy, Mines and Resources

Earth Physics Branch

Seismology Division

Ottawa, Canada

[1]Contribution from the Earth Physics Branch, No.:

ABSTRACT

Actual Fourier amplitude spectra of ground acceleration of
three northwestern United States earthquakes with epicenters with-
in several hundred kilometers of the Canada-U.S. border are com-
pared with theoretical spectra. In the theoretical treatment, a
conventional (deterministic) model of faulting is assumed and tra-
vel path complexities are restricted to attenuation and to the
free-surface reflection: the direct shear wave is considered to
carry most of the energy. Many of the principal features of actu-
al Fourier amplitude spectral curves can be adequately explained
by this technique but, for some events, there are indications of
an appreciable contribution from additional factors.

INTRODUCTION

A seismological interpretation of a velocity response spectrum of a single-degree-of-freedom oscillator, with low damping, subjected to strong ground motion such as that represented by an earthquake accelerogram is achievable by an indirect approach. The more basic Fourier amplitude spectrum of ground acceleration, which represents a lower limit to the velocity response spectrum of a low-damped (0% critical) oscillator, can, in principle at least, be associated directly with the seismic radiation from the causative fault, suitably modified by the structure of the travel path.

A unique physical interpretation of a response spectrum of a linear oscillator with small damping is difficult to attain for several reasons. First and foremost there is the intrinsic difficulty in separating the complexities introduced by travel path effects from the direct contribution from the source. The net result of this dilemma is that there is no consensus among seismologists as to the amount and mechanism of generation of high-frequency energy (Savage, 1972). Secondly a number of different types of fault models have been proposed (Haskell, 1964; Haskell, 1966; Savage, 1966; Aki, 1967; Archambeau, 1968; Brune, 1970).

The criterion used to select an appropriate model of faulting

to represent the source mechanism is governed by the availability
of published values for the associated fault parameters, given an
earthquake magnitude. The deterministic model of faulting of
Savage (1972) satisfies this requirement quite well and consequent-
ly is used in the present analysis. If we were to consider a more
realistic model of faulting (e.g. Savage, 1966) then we would re-
quire more information of fault parameters than is normally avail-
able to the seismologist.

EARTHQUAKE FAULT MODEL

The top diagram in Fig. 1 depicts the geometry of a vertical
strike-slip fault. Rupture initiates along a vertical line ele-
ment of extent W (fault width) and propagates horizontally in
opposite directions with a constant rupture velocity V_R. Rupture
extends over a fault length L, a distance L_o in the positive X_1-
direction and L_π in the opposite direction; that is, we are con-
sidering a bilateral form of a strike-slip fault, which is verti-
cal in this example. Without loss of generality, the direct shear
wave radiated in a vertical plane that passes through the origin
and is normal to the fault plane is considered. Travel path com-
plexities are restricted to intrinsic physical attenuation and to
the free-surface reflection.

Earthquakes that occur along a major fault tend, in general,
to have a similar fault mechanism whereas those that occur over a

broad area tend to have fault mechanisms that vary from region to region. Along the San Andreas fault in California, the mechanism is predominantly of the vertical strike-slip fault type. In that seismic region the direct shear wave is considered to carry most of the kinetic energy up to 100 km from the epicenter (Gutenberg, 1957). However, in the northwestern United States, the fault plane solutions of earthquakes tend to vary from region to region (Algermissen and Harding, 1965; Hodgson and Storey, 1954; Wickens and Hodgson, 1967; Crosson, 1972).

Table 1 shows fault plane solutions for two large earthquakes that occurred in Washington. The author is not aware of published fault plane solutions for the Helena, Montana earthquake. The preferred fault plane solutions for the Washington earthquakes are represented by the B-plane solutions (Hodgson and Storey, 1954; Algermissen and Harding, 1965). For the B-plane the plunge of the motion (slip) vector tends to be horizontal (2° and 21°), whereas for the A-plane the plunge tends to be vertical (78° and 55°). Strong motion records for these events tend to have a larger component in the horizontal plane rather than in the vertical plane (for examples see Trifunac et. al., 1973; Brady et. al., 1973). This would tend to favour the preferred (B) fault plane solutions because the plane of polarization of the direct shear wave would be nearly horizontal. Consequently, for these events the direct, horizontally polarized, shear wave is considered to

carry most of the kinetic energy as far as 100 km from the epi-
center. This assumption is similar to Gutenberg's (1957) con-
cept of the average California earthquake.

THEORY

DISPLACEMENT AMPLITUDE SPECTRUM

The shear-wave displacement amplitude density of the far-field
radiation pattern from a bilateral, vertical strike-slip fault as
formulated by Savage (1972) is

$$(1) \quad |U^S| = R_S(\phi, R) \cdot M_0 \cdot |\hat{G}| \cdot F_2(\omega, \tau_0, \tau_\pi) \cdot \omega$$

where R_S represents the radiation pattern at a polar angle ϕ
and a hypocentral distance R, M_0 the seismic moment, $|\hat{G}|$ the amplitude
spectrum of the source time function, F_2 the finiteness (in space)
of the source with delay times of τ_0 and τ_π in the positive and
negative X_1-directions respectively, and ω the angular frequency.

Respresentative values are assumed for the fault parameters
in Eq. (1) for a specified earthquake magnitude and distance and
are listed in Table 1. Since the emphasis is on strong ground
disturbances, we have selected unity (maximum value) for the value
of R_S, and this obtains when $\phi = \pi/2$. With this restriction the
fault plane is no longer vertical but is oriented so as to face
the detector on the surface. However, the mechanism is still
strike-slip, i.e. the plunge of the motion vector is essentially

zero (horizontal). The seismic moment as defined by Aki (1966) is

(2) $M_o = \mu S \bar{D}$

where μ is the shear modulus (or equivalently the modulus of rigidity), S the area of faulting (L x W) and $\bar{D}$ the average value of the relative displacement between opposite faces of the fault. The low-frequency energy is proportional to M_o, which is related to earthquake magnitude (Trifunac, 1972; Hasegawa, 1974). A ramp time function with a rise time T is assumed for the source time function G(t); the corresponding amplitude spectrum is (Haskell, 1966)

(3) $|\hat{G}(\omega)| = \dfrac{1}{\omega} \cdot \dfrac{1}{(1 + \omega^2 T^2)^{1/2}}$

Eq. (3) modulates the high-frequency part of the spectrum. In particular the factor containing T is constant at low frequencies and varies as ω^{-1} at frequencies above the corner frequency

(4) $\omega_2^c = T^{-1}$

The effect of the finite extent of the causative fault is represented by

(5) $F_2(\omega,\ \tau_o,\ \tau_\pi) = \left\{ \left[L_o F_{10} \right]^2 + \left[L_\pi F_{1\pi} \right]^2 + 2 L_o L_\pi F_{10} F_{1\pi} \cdot \cos(\omega \left[\tau_o - \tau_\pi \right] / 2) \right\}^{\frac{1}{2}} \cdot (L_o + L_\pi)^{-1}$

where L_o and L_π are as defined previously, $\tau_o = L_o/V_R$ and $\tau_\pi = L_\pi/V_R$, V_R being the rupture velocity, F_{10} and $F_{1\pi}$ are the familiar diffraction function. Thus

$$(6) \quad F_1 = \frac{\sin(\omega\tau/2)}{(\omega\tau/2)}$$

The spectrum for F_2 can be represented on a log-log plot by a flat spectrum at low frequencies and tends to oscillate about a high-frequency asymptote of slope -1 above a corner frequency ω_1^c where

$$(7) \quad \omega_1^c = \frac{2V_R}{L}$$

The geometric mean of ω_1^c and ω_2^c is represented by ω_3^c where

$$(8) \quad \omega_3^c = (\omega_1^c \cdot \omega_2^c)^{\frac{1}{2}}$$

ACCELERATION AMPLITUDE SPECTRUM

The Fourier amplitude spectrum of ground acceleration (FS) can be related to $|U^s|$ by (Trifunac, 1972; Hasegawa, 1974)

$$(9) \quad FS = |U^s| \cdot \omega^2 \cdot \exp(-\alpha R) \cdot 2$$

where $\alpha = \omega(2Q_s\beta)^{-1}$, $1/Q_s$ is a dimensionless measure of physical absorption $\frown$ and β is the shear wave velocity. The factor 2 takes into account the free-surface reflection. (Attenuation and the free-surface reflection could just as well have been incorporated with $|U^s|$.)

Actual FS curves are related to ground acceleration a(t) by

$$(10) \quad FS = \left| \int_0^{TW} a(t).\exp(-i\omega t).dt \right|$$

where TW is an appropriate measure of the duration of the strong

shaking part of the signal (usually near 30 sec). Note that FS

has the dimension of a velocity.

The relation that enables one to relate response spectrum to

the Fourier amplitude spectrum of ground acceleration, as calcu-

lated from Eq. (9) or derived from accelerograms by using Eq. (10),

is

$$(11) \quad FS \le SV_{0\%\zeta}$$

where SV is the velocity response of a single-degree-of-freedom

oscillator 0% critically damped (ζ) (Jenschke, 1970; Trifunac,

1972 (a)). Physically, FS represents the maximum velocity in a

single-degree-of-freedom oscillator of natural frequency $\omega/2\pi$ and

damping $0\%\zeta$ in the free vibrations following the passage of strong

seismic ground motion whereas $SV_{0\%\zeta}$ represents the maximum velo-

city in the same oscillator both during and after the passage of

the seismic vibrations.

Convenient ad hoc techniques are used to modify the shape of

theoretical FS curves at high frequencies so as to simulate the

shape of actual FS curves in this frequency range. This technique

is necessitated because of the inherent difficulty in separating

the contribution from the causative fault from that of the travel

path (scattering and attenuation). These ad hoc techniques are

implemented by the introduction of a constant Q_S in Eq. (9) in

some cases and a variable Q_S in others, i.e. a Q_S that varies with

the frequency of the wave.

GENERATION OF THEORETICAL FS CURVES

Fig. 1 shows, step-by-step, the various stages in the develop-

ment of theoretical FS curves, starting with the basic $\left| U^S \right|$ curve.

On a log-log plot the curve for $\left| U^S \right|$ can be represented by two

asymptotic trends, a low-frequency trend with a slope of zero and

a high-frequency trend with a slope of -2. The low-frequency trend

tends to increase approximately linearly with increasing earthquake

magnitude whereas the high-frequency trend tends to increase more

slowly. The reason for this is that the low-frequency asymptote

level depends upon seismic moment, the logarithm of which increases

approximately linearly with increasing magnitude whereas the high-

frequency trend tends to increase more slowly because ω_3^c tends

to decrease with increasing magnitude. There is no consensus

among seismologists as to the correct value of the slope of the high-

frequency asymptote; estimates range from -1 to -3. A multiplica-

tion of $\left| U^S \right|$ by ω effects a rotation in $\left| U^S \right|$, as can be seen in

the velocity amplitude spectrum. A further multiplication by ω

effects another rotation as shown in the acceleration amplitude

density curve. Two versions of FS curves are illustrated, one

with a constant Q_S (infinity in the case shown) and the other with

a variable Q_S. The bottom curve shows how Q_S varies with frequency.

The reason for selecting an upper corner frequency, which is represented by ω_4^c in this figure, in the frequency range 7-10 Hz is that many FS curves of California earthquakes manifest a sharp break in this frequency range. Moreover this corner frequency does not appear to correlate with either magnitude or distance.

The overall characteristics of actual FS curves (of predominantly California earthquakes) manifest contributions from sources other than those considered above. At low frequencies (0.05-0.1 Hz) there is generally evidence of a contribution from surface waves (fundamental Love and/or Rayleigh) because of a shallow focal depth. In addition, in regions where there is an appreciable deposit of low-velocity, unconsolidated sediments, there exist favorable conditions for the propagation of higher-mode surface waves at relatively higher frequencies (0.2-2 Hz). At intermediate frequencies (0.5-5 Hz) a contribution from complex crustal reverberations can be appreciable owing to constructive interference. We are not considering in any detail the feedback from building response, which can be considerable in this frequency range, especially for instruments deployed in the upper levels of high-rise buildings (for examples see Trifunac et al., 1973 a). Scattering of high-frequency waves by small-scale inhomogeneities in the upper part of the crust is very likely an important phenomenon, but seismologists so far have not been able to isolate this phenomenon in strong-motion records. Because we have neglected

all these complications in the theoretical treatment, we should

expect, a priori, that theoretical FS in general will provide a

lower limit to actual FS curves.

Table 1 shows the basic data input for the generation of

the theoretical FS curves shown in Figs. 2 to 5. The basic

source parameter required in generating a theoretical FS curve,

using the method outlined previously, is the seismic moment M_o

(see Eq.(2)) of an earthquake. Seismic moment is more accur-

ately evaluated from an analysis of surface waves (Rayleigh and/

or Love) rather than from body waves (P coda). This, in turn,

implies that the earthquake magnitude required in this analy-

sis is the surface wave magnitude M_s, suitably corrected for

focal depth, rather than the body wave magnitude m_b. There

are several reasons why we have elected to use the "M_s (effect-

ive)" magnitude rather than the reported (Gutenberg-Richter

scale) magnitude in the theoretical calculations. Firstly,

uncertainty in estimates of magnitude and focal depth of early

events (e.g. 1935 Helena, Montana earthquake - magnitude 6,

focal depth 40 km) would effect a very large spread or uncert-

ainty in the corresponding theoretical FS curve. Secondly, the

surface wave magnitude of later events (e.g. 1965 Puget Sound

earthquake) is not corrected for focal depth (Algermissen and

Harding, 1965). This correction factor depends upon focal

mechanism and can deviate appreciably from a linear dependence

upon focal depth (e.g. see Tsai and Aki, 1970). Thirdly, we are

dealing with one, and at the most, two stations for each event,

for which the radiation pattern value could differ appreciably

from the smoothed out or average value that obtains for the re-

ported magnitude.

To circumvent these problems, we arbitrarily fit the low-

frequency end of theoretical FS curves to the corresponding

portion of actual FS curves by perturbing the seismic moment.

This procedure appears feasible for relatively deep-focus (> 30 km)

events for which the surface-wave contribution in this spectral

range (for periods less than 20 s) is not likely to be sig-

nificant (e.g. see Hasegawa, 1974). Then using appropriate

tables or charts (e.g. Douglas and Ryall, 1972) that relate

seismic moment with earthquake magnitude, we can assign an

azimuthally dependent magnitude designated as M_s (effective) in

Table 1.

Incidentally the M_s (effective) magnitude for two of the

three events is related to the Gutenberg – Richter magnitude by

the Marshall and Basham (1972) empirical magnitude correction

formula of +0.008h, where h is the focal depth in kilometers.

This apparent deviation from the Marshall-Basham relation for

the Western Washington event is not surprising when we take into

consideration that magnitude at any specified station depends

upon the relative orientation of the station with respect to the

focal mechanism in addition to the focal depth. In any event, the M_s (effective) values listed in Table 1 are only ad hoc station values that are dependent upon the source mechanism and focal depth assumed for these events. For example, if the actual focal depth of the Helena, Montana event were much less that the value listed in Table 1, then the M_s (effective) value for this event would tend to decrease, that is approach the Gutenberg-Richter value.

COMPARISON BETWEEN THEORETICAL AND ACTUAL FS CURVES

Figures 2 to 5 depict, on a log-log plot, theoretical FS curves superimposed upon actual FS curves for the selected events. For the Western Washington earthquake, for which there are FS records at two epicentral distances, namely 17km and 57km, the theoretical curve was fitted to the actual curve corresponding to the shorter epicentral distance.

Fig. 2 is an illustration of a close fit between a theoretical and an actual (from Brady et al., 1973) FS curve for the Helena, Montana earthquake. The accelerogram from which the FS curve was derived was recorded by an instrument located on a concrete basement floor in contact with bedrock (Newmann, 1937). Because of the close correlation between the overall shape of theoretical and experimental FS curves, we can deduce the following information concerning the actual FS curve:

(1) surface waves (in the form of ground roll since the epicentral distance is too short to form properly developed surface waves) are present at frequencies less than 0.05 Hz (or

periods greater than 20 sec.).

(2)   a contribution from complex crustal reverberations in the mid-frequency range (0.3-5 Hz) appears to be relatively insignificant. The approximate near-vertical incidence of the direct wave tends to minimize signal perturbations owing to the presence of near-surface layering. The effect of the finiteness (size) of source (see. Eg. (5)) can explain the actual spectral shape in this frequency interval.

(3)   the close correlation at high frequencies between the theoretical FS curve for which a constant Q_s of 200 has been chosen and the actual curve implies the absence of appreciable scattering and dispersion. This again can be explained by the near-vertical incidence angle. Most of the travel path of the direct shear wave is through the comparatively more homogeneous part of the lower crust, in contrast to shallower-focus California earthquakes where the travel path is predominantly through the more heterogeneous upper crust.

Figs. 3 and 4 depict theoretical FS curves, with both constant and variable Q_s, superimposed upon actual (from Brady et al., 1973) curves for the Western Washington earthquake. The accelerograms were recorded on the first floor (Murphy and Ulrich, 1951). The fit between theoretical and actual FS curves is of intermediate quality for the close-in record (r = 17km) of Fig. 3 and of poorer quality for the more distant record (r = 57km) of Fig. 4. For the close-in record there is evidence of surface (Rayleigh)

wave energy for frequencies less than 0.05 Hz. In the mid-frequency range, i.e. 0.3-8 Hz, the theoretical curve with the smaller attenuation coefficient (larger Q_s) is a closer fit to the actual curve. The reason for this may lie in the fact that the direct wave is incident at the station at nearly vertical (13° from the vertical) incidence, with the consequence that the travel path is predominantly through the comparatively more homogeneous upper mantle and lower crust, rather than through the heterogeneous upper crust. In contrast to the close-in record, for which there is a reasonably good fit between theoretical and actual FS curves, the actual curve for the more-distance record tends to lie below the theoretical curves over the entire frequency range shown. Part of this discrepancy may be due to a variation in the radiation pattern ; part of it may be due to complexities in the near-surface layering near this station. Since the conspicuous peak near 1 Hz in the empirical FS curve is not present in the close-in record, this would indicate that it is not likely due the the assumed source. Constructive interference due to travel-path effects (near-surface crustal layering and/or local geology) may have effected this peak, which incidentally resembles peaks generated by building feedback (for example, see Trifunac et. al., 1973).

Fig. 5 is an example of a very poor fit in the intermediate-to-high frequency range between theoretical FS curves and an actual (from Brady et. al., 1973) curve for the Puget Sound earthquake.

The instrument was located in a Washington Highway Test Laboratory
(Brady et. al., 1973). As with the Western Washington earthquake,
surface waves are present for frequencies less than 0.05 Hz.
Although the curve with a variable Q_s results in a slightly better
fit than that for a constant Q_s there is, nevertheless, almost an
order-of-magnitude difference at intermediate-to-high frequencies
between theoretical and actual curves. Part of this discrepancy
may be due to an appreciable contribution from complex crustal
reverberations and from scattering in the near-surface layers.
Part of this discrepancy could be the omission of the compress-
ional (P) wave contribution in the theoretical FS spectrum.

In order to convert a complex problem into a tractable form,
we have imposed restrictions on source mechanism type and travel-
path complexities in the calculation of theoretical FS curves.
Consequently the physical interpretation given above of actual
FS curves of three northwestern U.S. earthquakes can be considered
a first order or an approximate interpretation. A more accurate
or quantitative interpretation would require the inclusion of
complexities introduced into the direct signal radiated from the
source by the crustal structure between source and detector and
the local geology under the detector. However, the inclusion of
crustal reverberations would generally require the use of numer-
ical techniques, which are generally very time consumming in con-

trast to the comparatively much shorter computer time required using the above-described analytic, but only approximate, technique. Even if a detailed knowledge of travel-path effects were attainable, the uncertainty in focal depth estimates of early events such as the 1935 Helena, Montana, earthquake effects an uncertainy in estimates of some of the physical parameters associated with the source. Suppose the actual focal depth of this event were less than the published value of 40 km by 10 or even as much as 20 km. Then the corresponding estimate of the source strength, namely seismic moment, would be less than that for the deeper focal depth. Consequently for some of the early events, uncertainties in estimates of focal depth would be the limiting factor in the interpretation of these events.

SUMMARY

(1) The similarity between theoretical and actual FS curves of the Helena, Montana earthquake implies that the direct shear wave carries most of the energy in this close-in record. Surface wave energy is present at frequencies less than 0.05 Hz (periods greater than 20 s). Because of the near-vertical incidence, crustal reverberations (in the mid-frequency range) do not appear to be appreciable.

(2) Surface wave energy is present at frequencies less than 0.05 Hz in FS records of the Western Washington and Puget Sound

earthquakes. In the mid-frequency (0.3-8 Hz) range, the FS components appear to experience a low attenuation, which may be due to the near-vertical incidence of the direct wave. To account for the discrepancy between theoretical and actual FS curves for the Puget Sound event, we must assume that multipathing together with possibly local geological effects are two of the primary contributors.

(3) In general theoretical FS curves tend to be below actual FS curves because of the omission of travel-path complexities and P-wave contributions in the theoretical computations. However, there is the odd case where the reverse occurs, such as the Western Washington event for r = 57 km. It is suggested that travel path complexities and radiation pattern effects may be two of the main contributors to this anomalous case.

BIBLIOGRAPHY

Aki, K. 1966. Generation and propagation of G waves from the
Niigata earthquake of June 16, 1964. Par II. Estimation of
seismic moment, released energy, and stress-strain drop from
the G-wave spectrum. Bull. Earthq. Res. Inst., Tokyo Univ.,
44, 73-88.

Aki, K. 1967. Scaling law of seismic spectrum. J. Geophys. Res.,
72, 1217-1231.

Algermissen, S.T. and Harding, S.T. 1965. The Puget Sound,
Washington Earthquake of April 29, 1965, Preliminary Seismo-
logical Report. U.S. Department of Commerce, Coast and Geo-
detic Survey, Rockville, Maryland.

Archambeau, C.B. 1968. General theory of elast^odynamic source
fields. Rev. Geophys. and Space Physics, 6, 241-288.

Brady, A.G., Trifunac, M.D. and Hudson, D.E. 1973. Fourier ampli-
tude Spectra, in Vol. IV, Part B, Earthq. Eng. Res. Lab.,
California Institute of Technology, EERL 73-100.

Brune, J.N. 1970. Tectonic stress and the spectra of seismic shear
waves from earthquakes. J. Geophys. Res., 75, 4997-5009.

Coffman, J.L. and von Hake, C.A. (editors) 1973. Earthquake
History of the United States, Publication 41-1. U.S. Depart-
ment of Commerce, National Oceanic and Atmospheric Administra-
tion.

Crosson, R.S. 1972. Small earthquakes, structure and tectonics of

the Puget Sound region. Bull. Seismol. Soc. Amer. 62, 1133-
1171.

Douglas, B.M. and Ryall, A. 1972. Spectral characteristics and
stress drop for microearthquakes near Fairview Peak, Nevada.
J. Geophys. Res., 77, 351-359.

Gutenberg, B. 1957. Effects of ground on earthquake motion. Bull.
Seismol. Soc. Amer., 47, 221-250.

Hasegawa, H.S. 1974. Theoretical synthesis and analysis of strong
motion spectra of earthquakes. Can. Geotech. J., 11, 278-297.

Haskell, N. 1964. Total energy and energy spectral density of
elastic wave radiation from propagating faults. Bull.
Seismol. Soc. Amer., 54, 1811-1842.

Haskell, N. 1966. Total energy and energy spectral density of
elastic wave radiation from propagating faults, 2, A statis-
tical source model. Bull. Seismol. Soc. Amer., 56, 125-140.

Hodgson, J.H. and Storey, R.S. 1954. Direction of faulting in
some larger earthquakes of 1949. Bull. Seismol. Soc. Amer.
44, 57-83.

Housner, G.W. 1959. Behavior of structures during earthquakes.
J. Eng. Mech. Div., Proceedings of the American Society of
Civil Engineers, 85, 109-129.

Housner, G.W. 1965. Intensity of earthquake ground shaking near
the caustive fault, in Proceedings of the 3rd World Conference
on Earthquake Engineering, 1, III-94-III-111.

Jenschke, V.A. 1970. Relations between response and Fourier spectra of shock functions. Int. J. of Solids and Structures, 6, 1259-1265.

King, CHI-YU, and Knopoff, L. 1968. Stress drop in earthquakes. Bull. Seismol. Soc. Amer. 58, 249-257.

Marshall, P.D. and Basham, P.W. 1972. Discrimination between Earthquakes and Underground Explosions employing an improved M_s Scale. Geophys. J. Roy. Astron. Soc. 28, 431-458.

Murphy, L.M. and Ulrich, F.P. 1951. United States earthquakes, 1949. U.S. Coast and Geodetic Survey, Serial No. 748.

Neumann, F. 1937. United States earthquakes, 1935. U.S. Coast and Geodetic Survey, Serial No. 600.

Nuttli, O.W. 1952. The Western Washington earthquake of April 13, 1949. Bull. Seismol. Soc. Amer., 42, 21-28.

Savage, J.C. 1966. Radiation from a realistic model of faulting. Bull. Seismol. Soc. Amer., 56, 577-592.

Savage, J.C. 1972. Relation of corner frequency to fault dimensions. J. Geophys. Res., 77, 3788-3795.

Trifunac, M.D. 1972. Tectonic stress and the source mechanism of the Imperial Valley, California, earthquake of 1940. Bull. Seismol. Soc. Amer., 62, 1283-1302.

Trifunac, M.D. 1972(a). Response Spectra, in Vol. III, Part A, Earthq. Eng. Res. Lab., California Institute of Technology Report EERL72-80.

Trifunac, M.D., Brady, A.G. and Hudson, D.E. 1973. Corrected accelerograms and integrated ground velocity and displacement curves, in Vol. II, Part B, Earthq. Eng. Res. Lab., California Institute of Technology, EERL 72-50.

Trifunac, M.D., Brady, A.G. and Hudson, D.E. 1973a. Fourier amplitude spectra, in Vol. IV, Part E, Earthq. Eng. Res. Lab. California Institute of Technology, EERL 73-109.

Tsai, Y.B. and Aki, K. 1970. Precise focal depth determination from amplitude spectra of surface waves, J. Geophys. Res., $\underline{75}$, 5729-5743.

Wickens, A.J. and Hodgson, J.H. 1967. Computer re-evaluation of earthquake mechanism solutions. Pub. Dom. Ob., Ottawa, Contribution number 103.

TABLE 1

Earthquake Parameters

Event	Helena, Mont.	W. Wash.	W. Wash.	Puget Sound
Date	31/10/35	13/4/49	13/4/49	29/4/65
Epicenter	$46°37'N$	$47°06'N$	$47°06'N$	$47°24'N$
	$111°58'W$	$122°42'W$	$122°42'W$	$122°18'W$
Magnitude[2]	6	7.1	7.1	6.5
M_s (effective)	6.3	7.1	7.1	7.0
M_o (dyne-cm)[3]	3.5×10^{25}	$8. \times 10^{26}$	$8. \times 10^{26}$	$2. \times 10^{26}$
L† (km)	10	50	50	35
W (km)	8	25	25	15
V_R (km/s)	3.4	3.4	3.4	3.4
D (cm) [4]	53	200	200	120
T (s)	0.5	0.5	0.5	0.5
h (km)	40 [5]	70 [6]	70	59 [7]
r (km)	3	17	57	61
R (km)	42	72	90	84

Fault plane Sol.

  A-plane

-strike	not available		$N28°E$	$N18°W$
-dip			$89°S$	$69°E$
-plunge of motion			$78°$	$55°$
vector				

TABLE 1 (cont'd)

B-plane

  -strike $N56^{o}W$ [8] $N53^{o}W$ [9]

  -dip $13^{o}S$ $35^{o}W$

  -plunge of motion 2° 21°

   vector

[2] reported magnitude (Housner, 1965;   Coffman and

                       von Hake, 1973)

[3] estimates for M_o are for M_s (effective)

[4] estimates are for M_s (effective) (Douglas and Ryall, 1972;

                          Hasegawa, 1974)

[5] (Housner, 1965)

[6] (Nuttli, 1952)

[7] (Algermissen and Harding, 1965)

[8] Preferred solution (Hodgson and Storey, 1954)

[9] Preferred solution (Algermissen and Harding, 1965)
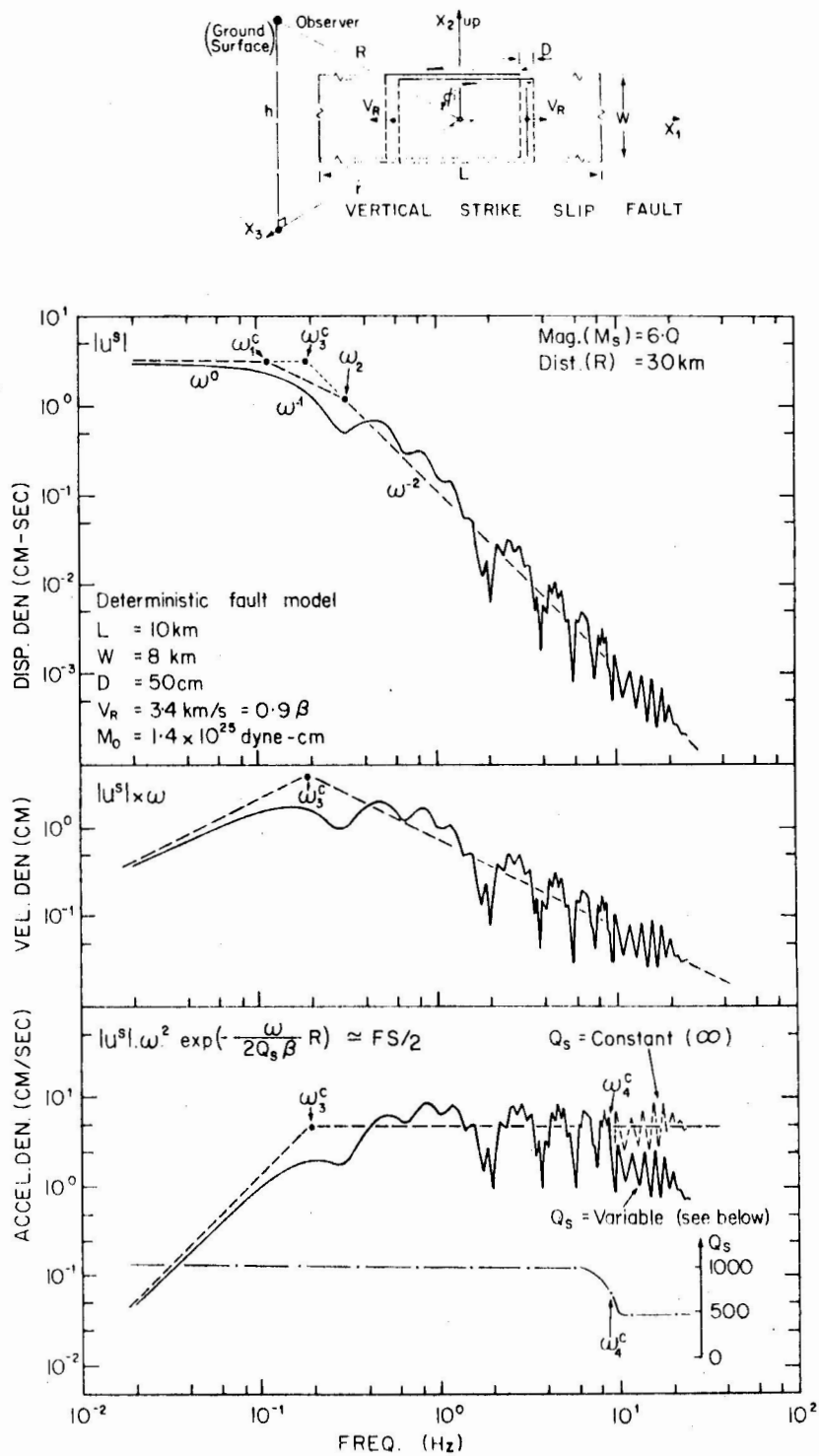
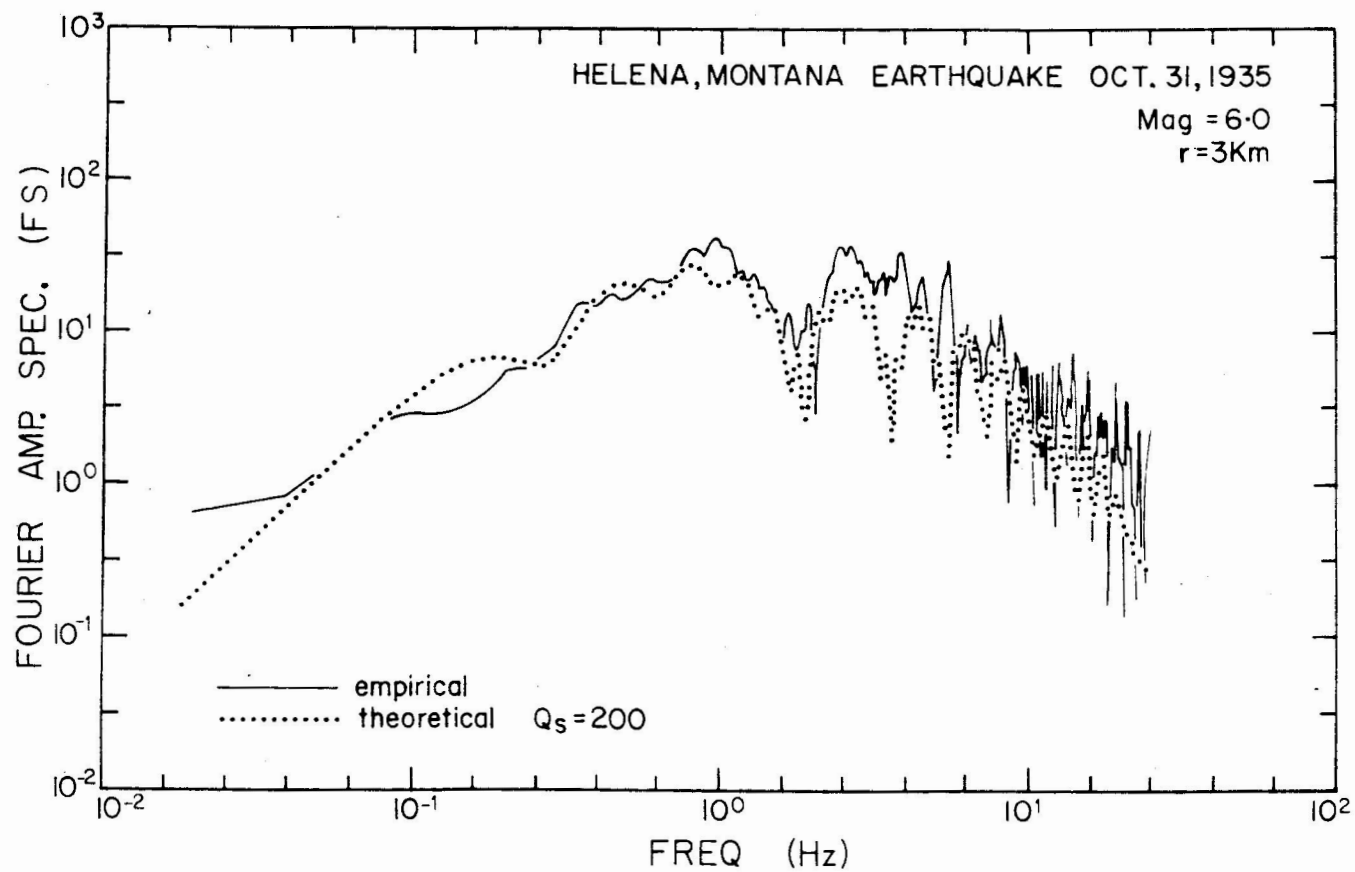FIG. 1   OUTLINE OF TECHNIQUE USED TO
GENERATE THEORETICAL FS
CURVES

FIG. 2   THEORETICAL FS CURVE SUPERIMPOSED UPON ACTUAL FS
CURVE OF HELENA, MONTANA, EARTHQUAKE.   THE ACTUAL
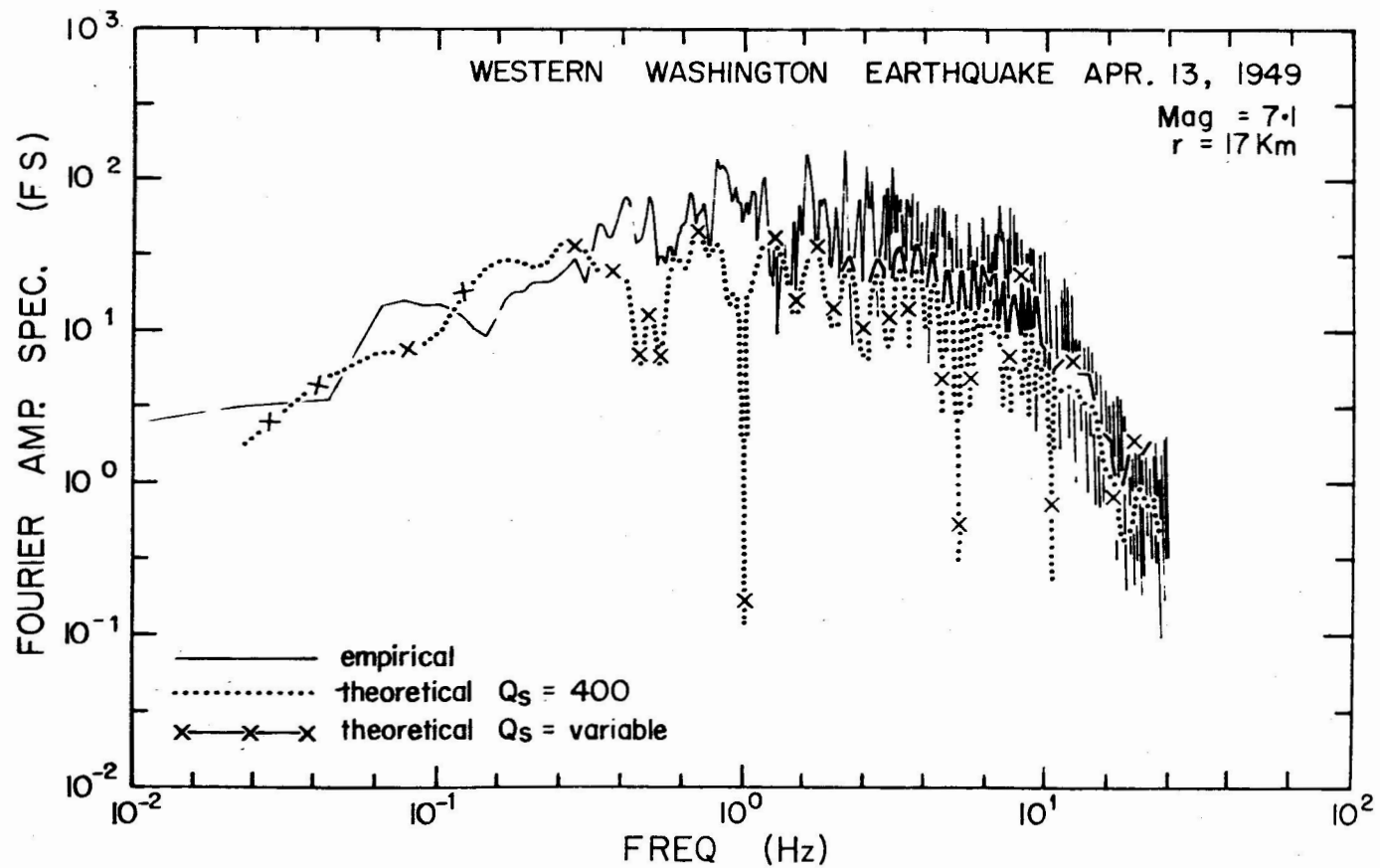FS CURVE IS FROM BRADY ET. AL. (1973)

FIG. 3   THEORETICAL FS CURVES WITH EITHER A CONSTANT OR A
VARIABLE Q_S SUPERIMPOSED UPON ACTUAL WESTERN
WASHINGTON EARTHQUAKE FS CURVES.   THE ACTUAL FS
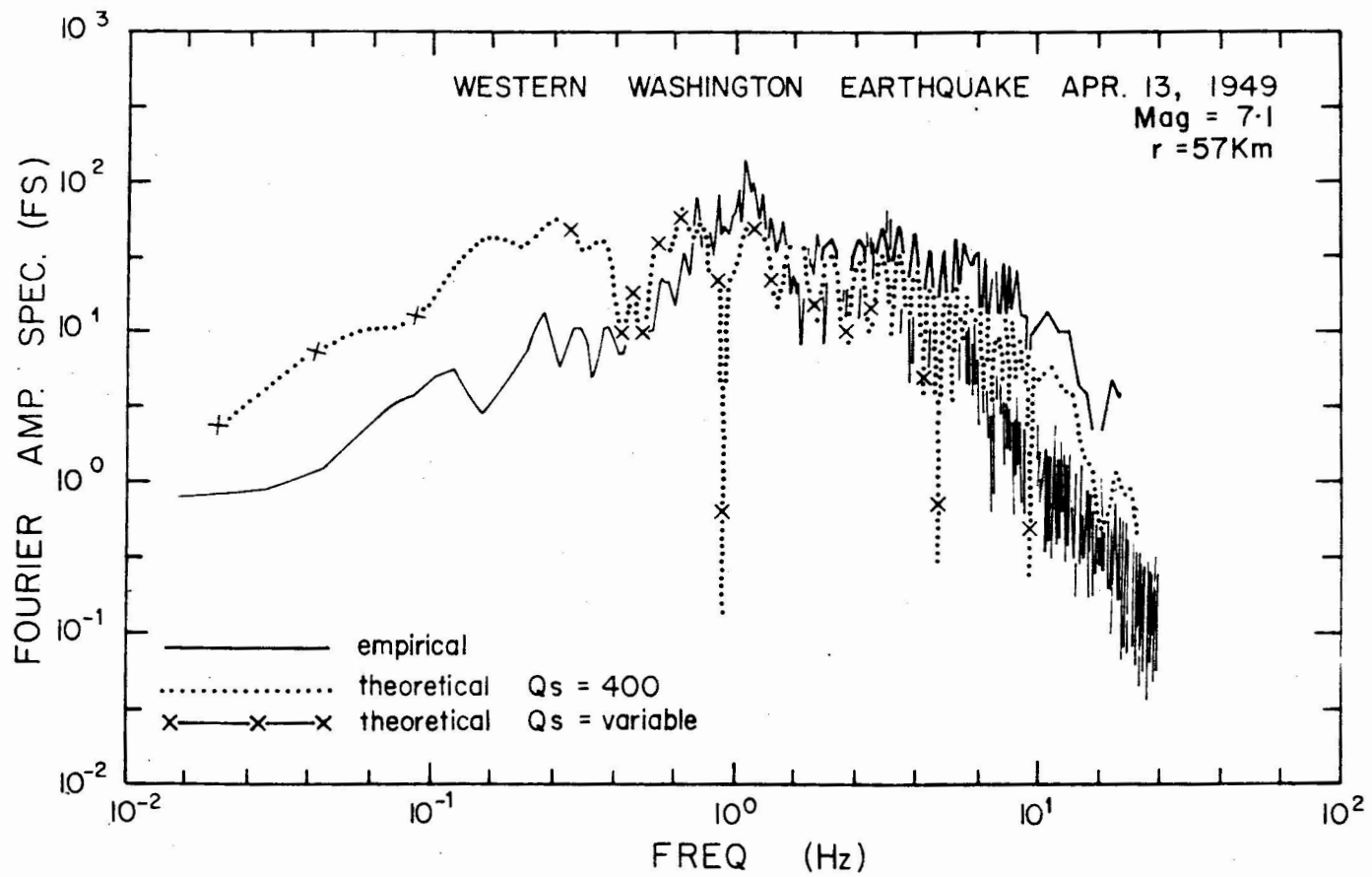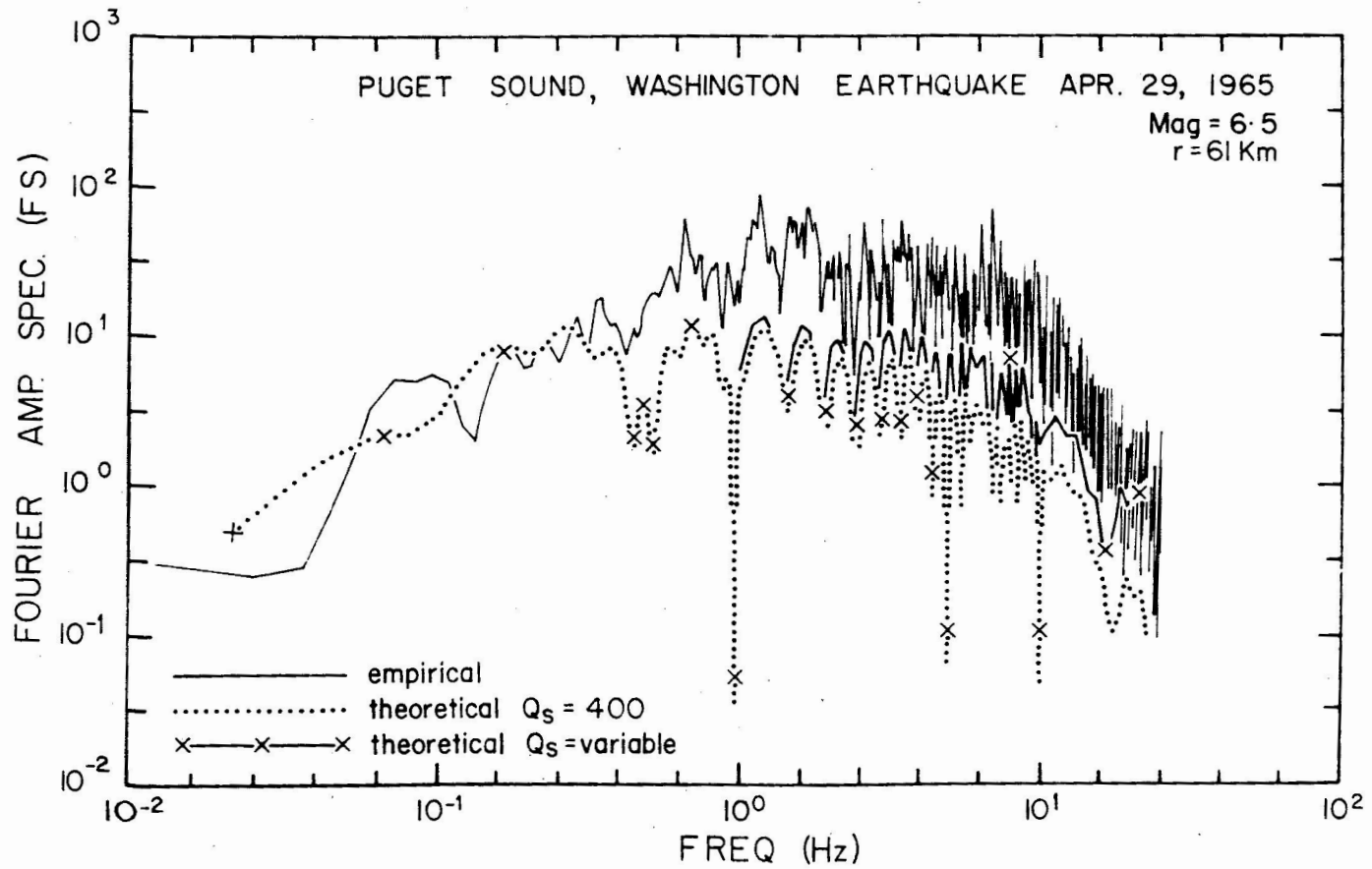CURVE IS FROM BRADY ET. AL. (1973)

FIG. 4   SAME AS FIG. 3 EXCEPT FOR DIFFERENT 'r'

FIG. 5   SAME AS FIG. 3 FOR PUGET SOUND EARTHQUAKE